Time-dependent solar modulation of cosmic rays from solar minimum to solar maximum

Bing-Bing Wang,[1,2] Xiao-Jun Bi,[1,2] Kun Fang,[1] Su-Jie Lin,[1] and Peng-Fei Yin[1]

[1]*Key Laboratory of Particle Astrophysics, Institute of High Energy Physics, Chinese Academy of Sciences, Beijing 100049, China*

[2]*School of Physical Sciences, University of Chinese Academy of Sciences, Beijing 100049, China*

(Received 17 April 2019; published 16 September 2019)

We study the time-dependent modulation effect and derive the local interstellar spectra (LIS) for the cosmic ray (CR) proton, helium, boron, and carbon. A two-dimensional modulation model including the variation of the interplanetary environment with time is adopted to describe the modulation process. The propagation equation of CRs in the heliosphere is numerically solved by the package Solarprop. We derive the LIS by fitting the latest results of several experiments, including Voyager 1, PAMELA, BESS-POLARII, and ACE, during low solar activity periods. We further study the modulation in the polarity reversal periods with the PAMELA proton data. We find that the rigidity dependence of the diffusion coefficient is critical to explain the modulation effect during reversal periods. Our results also indicate a power law relation between the diffusion coefficient and the magnitude of the heliospheric magnetic field at the Earth.

DOI: 10.1103/PhysRevD.100.063006

I. INTRODUCTION

After accelerated in sources, CRs are injected and propagated in the Galactic interstellar space. When entering the heliosphere, the intensities of CRs at low energies are significantly affected by several local effects, such as the interactions with the outward solar wind with an embedded magnetic field [1]. Therefore, the observed CR spectra are modulated with the solar activity cycle and are different from those outside the heliosphere, namely, the local interstellar spectra. The study of the solar modulation is essential, as it is indispensable for reproducing the low energy (<30 GeV) local interstellar spectra (LIS) and can also help us to understand the physical process in the CR-heliosphere interaction. The LIS are critical to determine the injection information and the propagation model of Galactic CRs [2–8], which are also closely related to some new physics studies, such as the indirect detection of dark matter [9–15].

The current data of CR experiments provide unprecedentedly good opportunities for the research of the solar modulation. Voyager 1, which has crossed the boundary of the heliosphere (heliopause) since August 2012, can give direct measurements of CR LIS from a few to hundreds MeV/nucleon [16–18]. Among the experiments, the PAMELA experiment [19,20] is particularly compelling for the study of solar modulation. The PAMELA Collaboration has published 8 years of CR data (07/2006–02/2014), continuously recording the variation of the CR proton spectrum from the late declining phase of solar cycle 23 to the maximum phase of solar cycle 24 [21,22]. Moreover, PAMELA performs precise measurements of the proton spectrum in a wide energy range of 80 MeV–50 GeV, partly overlapping with the energy range of Voyager 1. Then combining the results of PAMELA and Voyager 1, we can give good constraints on the model of solar modulation and obtain a reasonable CR proton LIS.

The most widely used model of solar modulation is the force-field approximation [23]. It is oversimplified to deal with all the current precise data. The more detailed models have been developed to interpret the observations [24–36]. In this work, we consider a time-dependent 2D modulation model including the diffusion, convection, drift, and adiabatic energy loss processes, to study the modulation effect over different solar activity periods and derive the CR LIS. Based on the public code Solarprop[1] [37], we numerically solve the propagation equation of CRs in the heliosphere with the stochastic differential equation approach. The typical parameters related to the interplanetary medium environment, such as the magnitude of the heliospheric magnetic field (HMF), the solar wind speed, and the tilt angle of the heliospheric current sheet (HCS), are taken from the observations. The scale factor of the diffusion coefficient is set to be a time-dependent free parameter to accommodate the observations.

In order to obtain the proton LIS in the form of cubic spline interpolation, we simultaneously fit the Voyager 1 data and the PAMELA data [18,21,38] in some low solar

[1]http://www.th.physik.uni-bonn.de/nilles/people/kappl.

activity periods. Then we attempt to explain the PAMELA results in the polarity reversal periods, which is more challenging compared with the case of less active periods. Besides, ACE and BESS experiments provide time-dependent spectra for CR nuclei [39–42], and Voyager 1 also measures the low energy LIS of CR nuclei [18]. We then derive the LIS of helium, boron, and carbon in the same framework with the study of a proton.

The paper is organized as follows. In Sec. II, we present the important ingredients describing the heliosphere environment. In Sec. III, we briefly describe the dominant physical mechanisms in the solar modulation effect. In Sec. IV, we drive the proton LIS using the PAMELA data and compare the calculated spectra with the PAMELA results over different solar activity periods. We also give an empirical relation between the diffusion coefficient and heliospheric magnetic field strength at the Earth. In Sec. V we present the LIS of helium, boron, and carbon. Finally, we give the summary in Sec. VI.

II. GLOBAL CHARACTERISTICS OF THE HELIOSPHERIC ENVIRONMENT

The CR propagation in the heliosphere is affected by the solar activity. The main factors that affect the CR transportation—namely, solar wind speed, the magnitude and orientation of the heliospheric magnetic field, and the inclination between the heliospheric current sheet and the equatorial plane, called the tilt angle—are all correlated with the solar activity.

The solar wind speed is variable in both latitude and time. During the solar minimum, the typical solar wind speed at the low latitude is about 400 km/s, while it increases by almost a factor of 2 at the high latitude [43]. With the increase of solar activity, the boundary of slow and fast solar wind rises rapidly [44]. The solar wind speed is described as [45]

$$V_{sw} = \begin{cases} V_{\max} & \theta \le 30^\circ \quad \text{or} \quad \theta \ge 150^\circ \\ V_{\min}(1+|\cos\theta|) & 30^\circ < \theta < 150^\circ, \end{cases} \tag{1}$$

where $V_{\max}$ is taken to be 760 km/s and $V_{\min}$ is the observation value near the Earth. For simplicity, we take the average latitude value as an approximation in this work.

The solar wind carries the Sun's magnetic field into the interplanetary space and forms the HMF with an Archimedean spiral structure given by [46]

$$\vec{B} = A\frac{B_0}{r^2}(\vec{e}_r - \tan\psi\vec{e}_\phi)(1-2H(\theta-\theta_{ns})), \tag{2}$$

where $A = +$ $(A = -)$ indicates the magnetic field polarity for the solar magnetic field lines pointing outward (inward) in the northern hemisphere and inward (outward) in the southern hemisphere, r is the distance from the Sun,

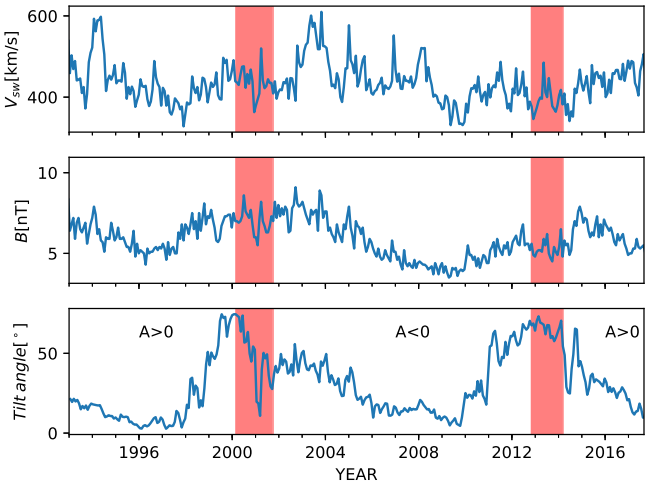

FIG. 1. Time profiles of the input interplanetary parameters in the solar modulation model. The top and middle panels show the solar wind speed and the magnetic field strength for each Carrington rotation taken from the OMNI website interface, respectively. The bottom panel represents the tilt angle of HCS taken from the WSO website with the "new" model. The red boxes represent the estimated polarity reversal periods [50,51].

$B_0\sqrt{(1+\tan^2\psi(r=1\ \text{AU},\theta=\pi/2))}$ is the magnetic field magnitude at the Earth, H is Heaviside function, θ is the polar angle, and V_{sw} is the solar wind speed. The spiral angle ψ is defined as $\tan\psi = \frac{\Omega r\sin\theta}{V_{sw}}$, where $\Omega = 2.866\times10^{-6}$ rad/s is the rotation speed of the Sun. Note that θ_{ns} determines the position of the heliospheric current sheet (HCS), which divides the heliosphere into two regions with opposite polarities. The structure of the HCS is parametrized by its tilt angle and is well related to the solar activity. Some modifications of the Parker HMF have been proposed in [47–49] but remain inconclusive. We adopt the standard Parker HMF model in this work.

In Fig. 1 we show the time profile of the parameters characterizing the global heliospheric environment in our model. The first and second panels show the averaged solar wind speed (V_{sw}) and HMF magnitude at 1 AU (B_E) using the data from the OMNI website interface[2] for each Carrington rotation (about 27.28 days), respectively. The third panel illustrates the variation of the tilt angle (α) taken from the WSO website[3] with the "new" model. The estimated periods of changeover of the solar magnetic polarity [50,51] are represented by the red bands. During the time period considered in this work, the solar wind speed and the magnetic field magnitude near the Earth vary in the ranges of 328–610 km/s and 3.1–9.1 nT, respectively. The tilt angles have an obvious variation

[2]omniweb.gsfc.nasa.gov.
[3]wso.stanford.edu.

from 4.5° to 74.5°. Both the HMF strength and tilt angle show a clear nearly 11-year cycle.

As shown in Fig. 1, the description for the heliosphere environment with fixed parameters is not realistic. In the original Solarprop, not only the magnetic field strength but also the tilt angle change with time. We further extend the code to allow the variation of solar wind speed. In this work, we study the solar modulation effect including a smooth time correlation to the solar activity. As a valid approximation, the input parameters are averaged over the timescale of the solar wind propagation from the Sun to the modulation boundary.

III. CR PROPAGATION IN THE HELIOSPHERE

The CR propagation within the heliosphere is dominantly affected by four effects, including the diffusion induced by scattering magnetic irregularities, the convection caused by outward solar wind, the drift induced by the irregularity of the global heliosphere magnetic field, and the adiabatic energy loss [52]. The modulation effect in the heliosheath is neglected here. For the discussion of this possible effect, we refer the reader to [53–55]. The review of the solar modulation can be found in [52,56].

The CR propagation within the heliosphere can be described by the Parker transport equation [1]:

$$\frac{\partial f}{\partial t} = -(\vec{V}_{sw} + \vec{V}_{\rm drift}) \cdot \nabla f + \nabla \cdot [K^s \cdot \nabla f] + \frac{\nabla \cdot \vec{V}_{sw}}{3} \frac{\partial f}{\partial \ln p}, \tag{3}$$

where $f(\vec{r}, p, t)$ is the omnidirectional distribution function, $\vec{r}$ is the position in a heliocentric spherical coordinate system, p is the particle momentum, $\vec{V}_{sw}$ is the solar wind velocity, $\vec{V}_{\rm drift}$ is the drift velocity, and K^s is the symmetric part of the diffusion tensor. The differential intensity related to the distribution function is given by $I = p^2 f$.

We are far from completely understanding the parametrization of the diffusion tensor [30,57–59]. In this work, a simple spatial and rigidity dependence of the parallel diffusion coefficient $K_\parallel$ is adopted as follows [37]:

$$K_\parallel = \begin{cases} \frac{1}{30} k\beta \frac{B_E}{B} & R < 0.1 \text{ GV} \\ \frac{1}{3} k\beta \frac{R}{R_0} \frac{B_E}{B} & R \geq 0.1 \text{ GV} \end{cases} \tag{4}$$

where $k \equiv k_0 \cdot 3.6 \times 10^{22}$ cm^2/s is a scale factor, which describes the time dependence of the diffusion coefficient and reflects the variability of interplanetary medium properties, B_E is the strength of the HMF at the Earth, B is the strength of the HMF at the particle position, and R is the rigidity with $R_0 = 1$ GV. This rigidity dependence is suggested for modulation during the solar minimum in [60] based on the quasilinear theory [61]. For particle rigidity above a threshold value the linear rigidity dependence of the diffusion coefficient is commonly adopted in many works [23,45,62–66]. The diffusion coefficient perpendicular to the large scale HMF $K_\perp$ is taken to be $K_\perp = 0.02 K_\parallel$ according to the test particle simulation [67]. This form of $K_\perp$ is widely adopted in the literature [31,68].

The drift effect leads to a charge-sign dependence and a 22-year cycle in the solar modulation effect [69–71]. The drift velocity from the gradient and curvature of the HMF is written as $\vec{V}_{gc} = q\frac{\beta R}{3} \nabla \times \frac{\vec{B}}{B^2}$ [70]. The HCS drift is caused by the change of the field direction at the crossing of the HCS. In this study, we describe the HCS drift following [72], where a thick, symmetric transition region determined by the tilt angle is used to simulate a wavy neutral sheet. Combining the $\vec{V}_{gc}$ and effective wavy neutral sheet drift velocity $\vec{V}^w_{ns}$ shows that the drift velocity is divergence-free in the region of $\pi/2 - \alpha - \theta_\triangle < \theta < \pi/2 + \alpha + \theta_\triangle$, where $\theta_\triangle \approx \frac{2RV_{sw}}{AB_0\Omega\cos\alpha}$. The $\vec{V}^w_{ns}$ is given by

$$\vec{V}^w_{ns} = \begin{cases} qA\frac{v\theta_\triangle \cos(\alpha)}{6\sin(\alpha+\theta_\triangle)}\vec{e}_r & \pi/2-\alpha-\theta_\triangle < \theta < \pi/2+\alpha+\theta_\triangle \\ 0 & \text{else} \end{cases} \tag{5}$$

where q is the charge sign and v is the particle speed. The product of qA determines the drift direction. During the $A < 0$ cycle the positive charge particles drift inwards mainly through the HCS near the equatorial regions. Otherwise, during the $A > 0$ cycle, they mainly drift inwards from polar regions.

In this work, we use the public Monte Carlo code Solarprop [37] to numerically solve the transport equation. The computation is based on the equivalence of a set of stochastic differential equations to the Parker equation. For the details of the numerical method, we refer the reader to [37,73–75]. We take the termination shock as the modulation boundary and assume that it is 100 AU from the Sun. In our default calculation, the only free parameter is the time-dependent scale factor of the diffusion coefficient k_0. Other input parameters are obtained from observations, such as the solar wind speed, the magnitude of the magnetic field, and the HCS tilt angle.

IV. SOLAR MODULATION FOR PROTONS

The PAMELA experiment performed a systematic measurement of the CR proton spectrum in the period 2006–2014 from the late declining phase of solar cycle 23 to the maximum of cycle 24. The detailed comparison between the calculated energy spectra and the observations for different solar activity levels can improve our understanding of the modulation process.

TABLE I. The parametrization of proton LIS with cubic spline interpolation.

$\log(E_k/\mathrm{GeV})$	−2.42	−1.41	−0.50	0	0.50	1.00	1.50	2.00
$\log(I/(\mathrm{GeV\,m^2\,sr\,s}))$	4.3003	4.4676	4.0396	3.4675	2.5702	1.4101	0.0685	−1.3465

A. Local interstellar spectrum for protons

The Voyager 1 crossed the heliopause on August 2012 and provided the CR LIS at very low energies. Additionally, the CR spectra measured by PAMELA and AMS-02 with rigidity above a few tens of GV are not affected by the modulation. However, until now, there have been no experiments to measure the LIS in the gap. To derive the LIS we parametrize the LIS with the cubic spline interpolation method [76,77]. We obtain the proton LIS by fitting the calculated spectra to the Voyager 1 observation and a series of PAMELA data. The GNU Scientific Library (GSL)[4] is used to perform the least-squares fitting. In order to avoid the influence of the polarity reversal that occurred in late 2012, the PAMELA sample data are chosen between July 2006 and February 2012. For considerable savings in computing time we use 12 sets of data to construct the LIS. The corresponding Carrington rotation numbers of the data used in the fit are 2045, 2052, 2058, 2064, 2070, 2076, 2082, 2088, 2093, 2107, 2114, 2121.

The knots and the corresponding proton intensities are listed in Table I. Figure 2 shows the obtained proton LIS and the experimental results, including the Voyager 1, PAMELA, and AMS-02 data [18,78,79]. The LIS agrees with the proton flux measured by Voyager 1 outside the heliosphere at low energies below 300 MeV and is consistent with the data measured by PAMELA and AMS-02 at high energies above a few 10 GeV. The LIS shows that it is less affected by the solar modulation for protons above 10 GeV.

In this analysis, we derive LIS with the cubic spline interpolation method. Note that other forms of LIS are also possible. For instance, in the plain diffusion scenario, the break in the injection spectrum or the diffusion constant at a few GV would lead to a LIS with the broken power law form. When more propagation effects are considered, such as reacceleration or convection, the predicted LIS becomes more complex and would depend on the choice of these propagation effects. We have checked that the difference between the LIS derived with the broken power law form above 1 GeV and the cubic spline interpolation method is at most 5% in a wide energy range.

B. Comparing the calculated proton spectra with the observations before the polarity reversal

After deriving the proton LIS, we can calculate the modulated proton spectra in different periods and compare them to the spectra observed by PAMELA. We first focus on the modulation before the polarity reversal. The northern and southern polar fields were reversed in November 2012 and March 2014, respectively [51]. In every period, the diffusion coefficient is adjusted to reproduce the observed PAMELA spectrum in the range of 0.08–40 GeV.

In Fig. 3, we show that our calculated proton spectra are consistent with the corresponding PAMELA data over a wide energy range in 8 different periods. The time evolution of the proton flux is closely related to the solar activity. The proton flux gradually increased from 2006 to 2009 until reaching the maximum value during December 2009; it then decreased from 2010 to 2012. We also show the time profile of reduced-χ^2 (χ^2/d.o.f.) in the fit to the PAMELA data on a solar rotation period basis in Fig. 4. Figure 4 also indicates that χ^2 after 2011 has larger values than those before 2011. We find that the reduced-χ^2 in all the fits is much smaller than 1. This indicates that our calculated spectra are consistent with the observations. However, it should be noted that such small χ^2 may be underestimated due to the correlations of the systematic uncertainties. In this work, the impact of this effect is not taken into account. Related studies can be found in Refs. [80–82].

C. Modulation in the polarity reversal period

Although the calculated proton spectra show a good agreement with the PAMELA observations in the periods 07/2006 and 10/2012, there are large discrepancies in the

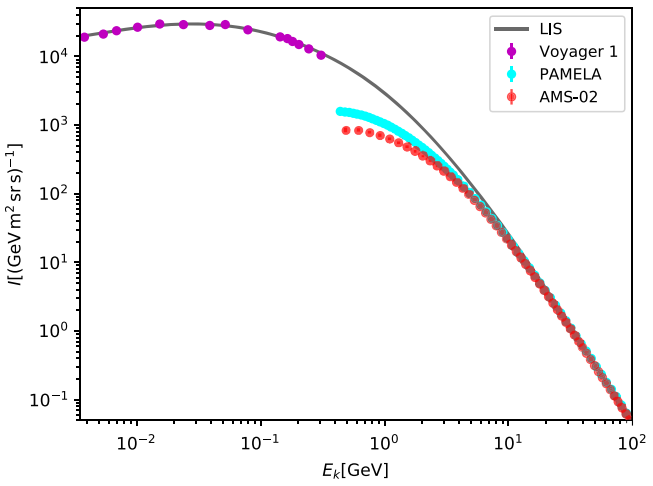

FIG. 2. Comparison of the proton LIS to the observations. The grey curve represents the proton LIS. The purple, cyan, and red dots represent the Voyager 1, PAMELA, and AMS-02 data, respectively.

[4]https://www.gnu.org/software/gsl.

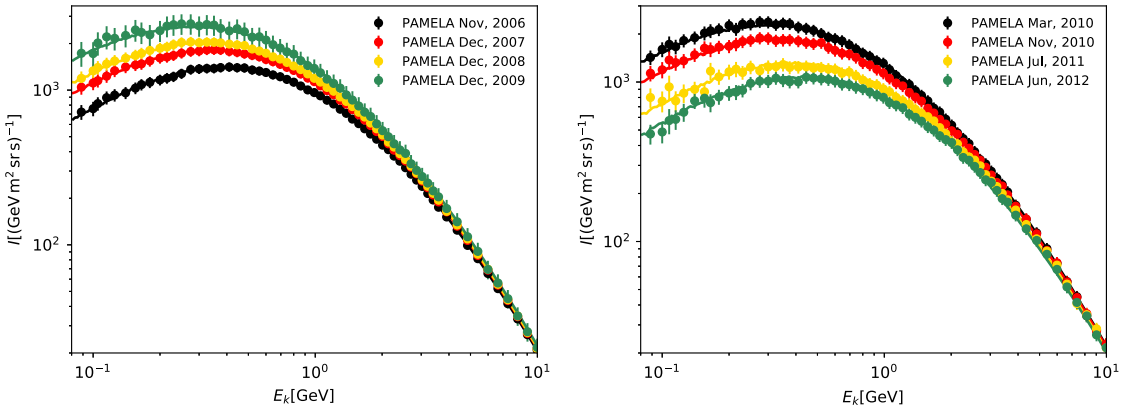

FIG. 3. The calculated proton spectra (solid lines) are compared to a selection of the PAMELA data (dots) in 2006–2009 (left panel) and 2010–2012 (right panel).

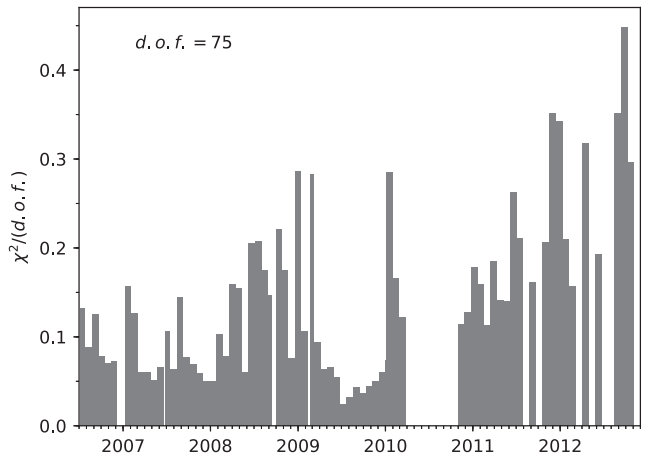

FIG. 4. The time profile of reduced-χ^2 from the fit to the PAMELA proton data during 07/2006 to 10/2012.

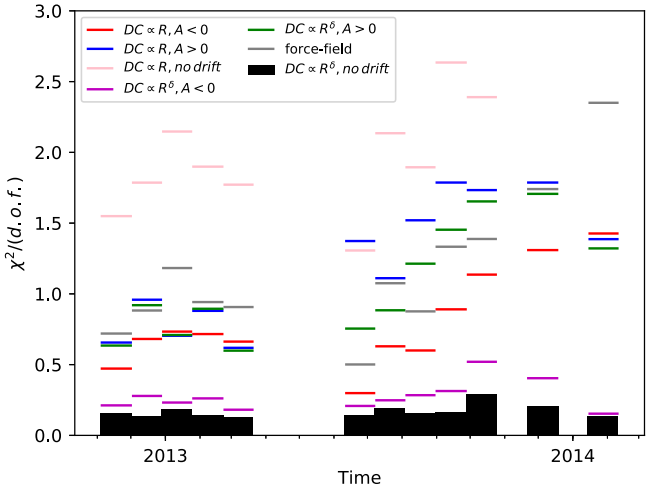

FIG. 5. Reduced-χ^2 from the fits to the PAMELA proton data in the polarity reversal periods for the force-field approximation model and six assumptions on the diffusion coefficient and drift effect.

subsequent polarity reversal period. The polarity reversal often occurs near the solar maximum.

It is a challenge to model the modulation effect in the polarity reversal period. The gradual reversal process and the frequent solar events disturb the interplanetary medium; therefore, the magnetic field structure becomes more complex in this period. The diffusion and drift coefficients related to the Parker magnetic field model might not be appropriate during the polarity reversal period. To account for this fact, we modify the diffusion coefficient by introducing a power law rigidity dependence. The diffusion coefficient is described as $k_\perp \propto k_\parallel \propto R^\delta$ (DC $\propto R^\delta$) for the particle rigidity above 0.1 GV. We take δ as a free parameter rather than a constant 1 in our default case. Some studies argue that the drift effect vanishes during the solar maximum [83,84]. We attempt to turn off the drift effect in our model.

We make some assumptions for the modulation effect in the polarity reversal periods. There are two assumptions for the rigidity dependence of the diffusion coefficient: $DC \propto R$ and $DC \propto R^\delta$. For the drift effect, we consider

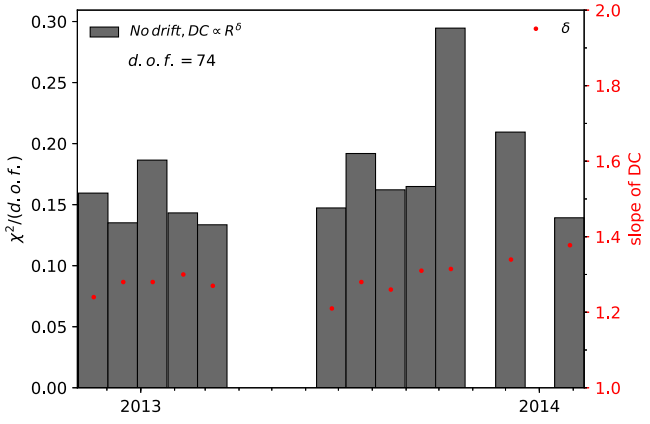

FIG. 6. The time profile of reduced-χ^2 and the slope of diffusion coefficient δ from the fit to the PAMELA proton data during the polarity reversal periods.

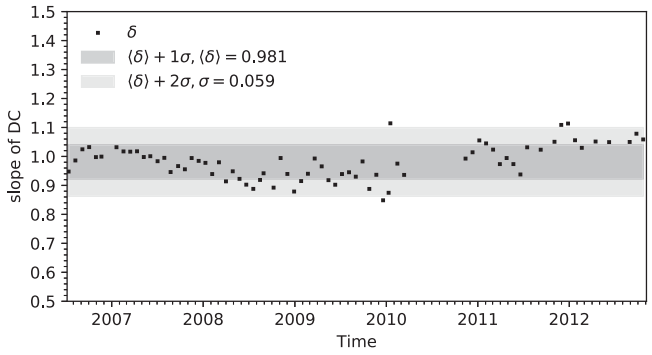

FIG. 7. The time profile of δ before the polarity reversal.

three cases: the polarity is positive ($A > 0$), the polarity is negative ($A < 0$), and there is no drift effect. Thus there are a total of six assumptions for the diffusion coefficient and drift effect. The force-field approximation model is also included in our comparison. In Fig. 5 we show the resulting χ^2 from the fits to the PAMELA proton data for different scenarios. We find that the assumption with a $DC \propto R^{\delta}$ and without drift provides the best fit. It is evident that adopting the power law rigidity dependence of the diffusion coefficient can significantly reduce χ^2. The time profile of δ and reduced-χ^2 for the best fit are shown in Fig. 6. We also check the assumption of the linear rigidity dependence ($\delta = 1$) before the polarity reversal. We get the mean and standard deviation as 0.981 and 0.059, respectively. From the time profile of δ shown in Fig. 7, it can been seen that $\delta = 1$ is a good approximation. As the diffusion coefficient is related to the magnetic field power spectrum, the property of the HMF turbulence during polarity reversal should be different in the quiet epochs.

D. Empirical relation between the diffusion coefficient and the magnitude of HMF at the Earth

It is well known that the diffusion coefficient is anticorrelated with HMF strength. In this work, the time dependence of the diffusion coefficients is described by a scale factor $k_0(t)$. The time variations in magnetic field strength are introduced by averaging B_E over the time taken for the solar wind to reach the modulation boundary from the Sun. Figure 8 shows the time profile of $k_0(t)$ and backward time average of the HMF at the Earth $\langle B_E \rangle$.

We follow the previous works [85,86] and assume $k_0 = (\frac{B_c}{\langle B_E \rangle})^n$, where B_c and n are free parameters. Figure 9 shows the relation between k_0 and $\langle B_E \rangle$ during 07/2006 and 02/2013. For the period of 06/2013–02/2014, the correlation between k_0 and $\langle B_E \rangle$ is weak (see Fig. 8), so we do not take into account this period. Obviously there is a discrepancy between B_c in the declining phase (07/2006–03/2010) and in the increasing phase (10/2010–02/2013) of the observed cosmic ray intensity level, while we find that the power n is approximately 2 and slightly varies with time. This result is consistent with the

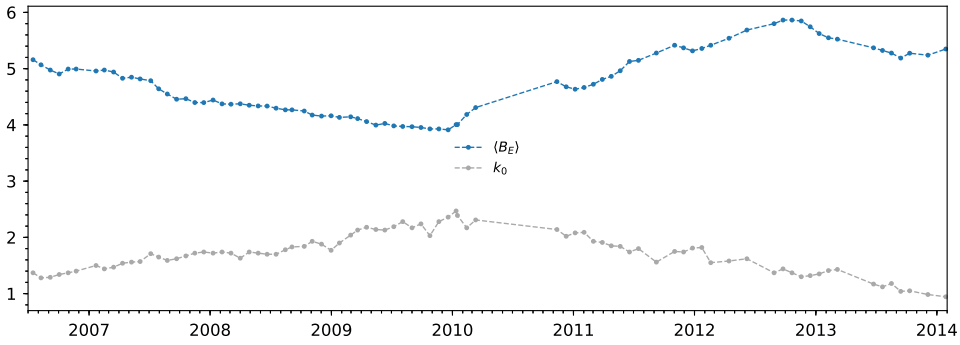

FIG. 8. The time profile of k_0 and the backward average of the HMF strength $\langle B_E \rangle$.

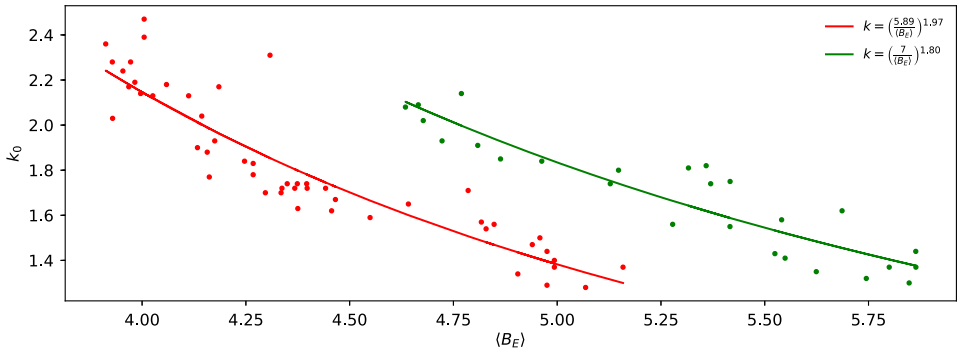

FIG. 9. The power law relation between the diffusion coefficient k_0 and the average HMF strength at the Earth $\langle B_E \rangle$. The red and green lines represent the fitting results during 07/2006 to 03/2010 and during 10/2010 to 02/2013, respectively.

TABLE II. The parametrization of the LIS spectrum for helium, boron, and carbon with the cubic spline interpolation method.

	$\log(R/\mathrm{GV})$	−1.0	−0.50	0	0.50	1.00	1.50	2.00
He	$\log(I/(\mathrm{GeV\,m^2\,s\,sr}))$	2.4742	2.7412	2.6561	1.7645	0.4564	−0.8996	−2.2882
B	$\log(I/(\mathrm{GeV\,m^2\,s\,sr}))$	−1.5451	−0.6089	−0.3095	−0.7162	−3.5311	−5.0564	−6.6083
C	$\log(I/(\mathrm{GeV\,m^2\,s\,sr}))$	−0.7080	0.2617	0.4494	−0.3155	−1.5787	−2.9170	−4.2698

conclusion in [87]. From the empirical relation found in the fit, we can use the estimated magnetic field strength to obtain the diffusion coefficient and get predictions for the modulated spectra.

The different relationships between the diffusion coefficient and solar parameters for the ascending and descending phases have been discusses in several works, e.g., [29,45,88]. In [29,45], the authors expressed the diffusion coefficient k_0 as a function of the monthly smoothed sunspot number. With the same sunspot number, k_0 is larger during the ascending phase than during the descending phase. In [88], the authors studied the relation between the annual modulation potential and the solar open magnetic flux. However, the physical reason for these different behaviors remains unclear. Further studies are needed to give a conclusive interpretation.

V. LIS FOR HELIUM, CARBON, AND BORON

In order to derive the LIS for other nuclei, we investigate the modulation effect for the CR helium, boron, and carbon. Here, we also use the cubic spline interpolation method to construct the LIS and derive the helium LIS by minimizing the weighted differences between the calculated spectra and the observations of Voyager 1 and BESS-POLARII. The same method is used but with the combination of data from the Voyager 1, PAMELA, and ACE boron (carbon) observations in 2009 to obtain the boron (carbon) LIS. The parameters of the LIS are summarized in Table II.

In Fig. 10 we show the calculated CR helium spectra and compare them with the AMS-01, BESS98, BESS-POLARI, and BESS-POLARII results [41,42,89]. The LIS of helium and the Voyager 1 data are also shown. In order to reproduce the spectra observed by AMS-01, a factor of 1.25 is adopted to scale down the LIS. Figures 11 and 12 show

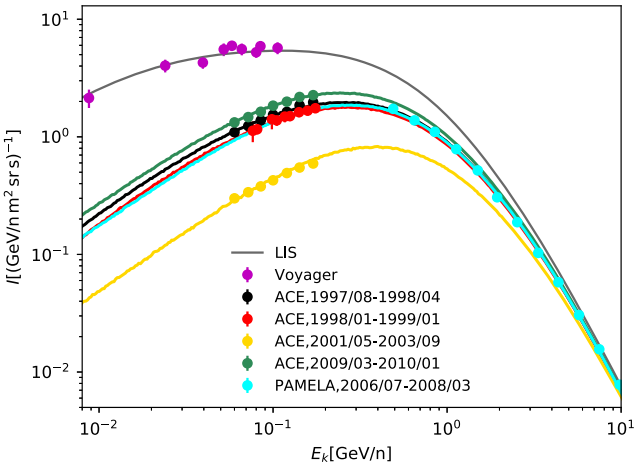

FIG. 11. The calculated boron spectra compared to the experimental observations, including Voyager 1, ACE, and PAMELA results.

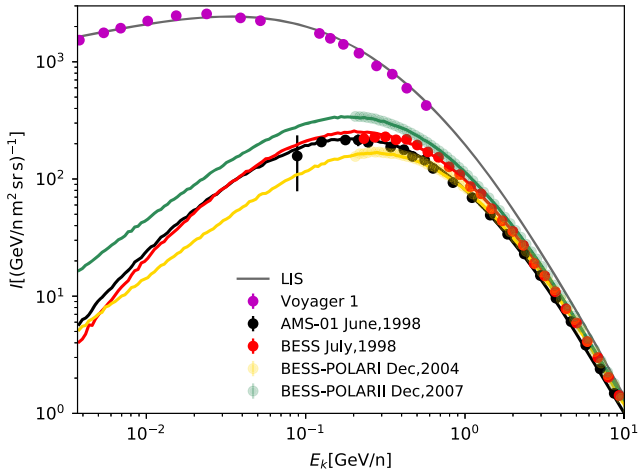

FIG. 10. The calculated helium spectra compared to the experimental observations, including the Voyager 1, AMS-01, and BESS results.

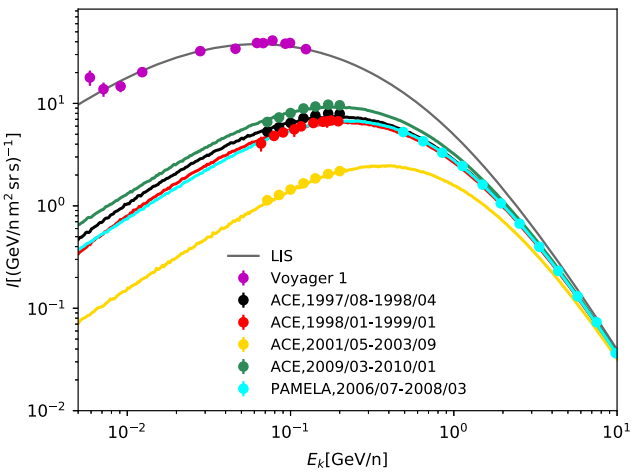

FIG. 12. The calculated carbon spectra compared to the experimental observations, including Voyager 1, ACE, and PAMELA results.

the LIS and calculated spectra for boron and carbon, respectively. For comparison, the ACE and PAMELA results [39,40,90] are also shown. We see that our calculated spectra can reproduce the observations well. Note that in our calculation, the CR spectra for different nuclei in the same period share modulation parameters. This is an important improvement compared with the force-field approximation model, where the potential parameter should be specified for each CR species [40].

VI. CONCLUSION

In this work, we study the solar modulation of CRs and derive the new CR LIS with a time-dependent modulation model and the latest CR experiments. The parameters describing the global characteristics of the heliospheric environment, such as the solar wind speed, magnetic field magnitude, and tilt angle, are all obtained from observations. In our default calculation, the only free parameter is the scale factor of the diffusion coefficient.

We adopt the long-term PAMELA observation to derive the LIS and investigate the modulation effect of the CR proton. We utilize some data samples of PAMELA during the low solar activity periods and the result of Voyager 1 to obtain the proton LIS; then all the PAMELA data before the polarity reversal can be well reproduced. Modeling the modulation effect during the polarity reversal period is challenging since the theory of CR propagation in the heliosphere during this period is poorly understood. The complex magnetic field configuration increases the uncertainties of diffusion and drift effects. In order to reproduce the observations, we change the linear relation between the diffusion coefficient and rigidity to $DC \propto R^{\delta}$ and assume there is no significant drift effect in the polarity reversal period. We find that the diffusion coefficient is anticorrelated to the HMF strength at the Earth. An empirical relation can be described as $DC \propto \langle B_E \rangle^{-n}$, where n is ~ 2 and slightly varies with time.

We also study the modulation effect and derive the LIS for the CR helium, boron, and carbon. In the calculations, the parameters in the modulation model are taken to be the same for different CR species in the same period. Since the calculated spectra can well explain several experimental results, our approach is a good description for dealing with the modulation effect. Using the LIS derived here, uncertainties in the study of the CR propagation in the Galaxy can be reduced.

ACKNOWLEDGMENTS

This work is supported by the National Key R&D Program of China (Grant No. 2016YFA0400200) and the National Natural Science Foundation of China (Grants No. U1738209 and No. 11851303).

APPENDIX: COMPARISON WITH THE FORCE-FIELD APPROXIMATION

In order to compare our results with the force-field approximation, we show the difference of χ^2 from the fits to the long-term PAMELA proton observations in two scenarios in Fig. 13.[5] We can see that in most periods the force-field approximation gives a larger χ^2 than our results.

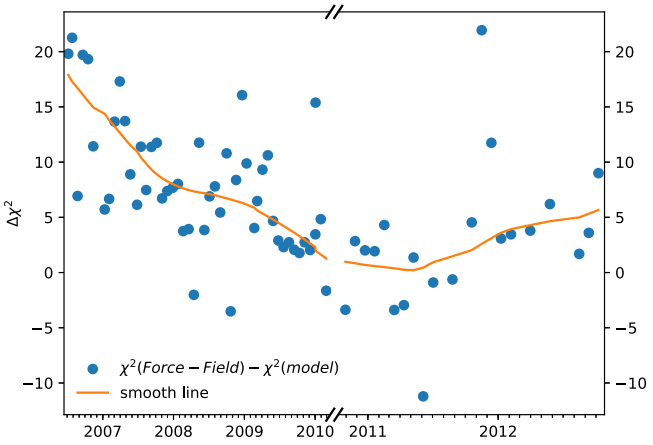

FIG. 13. Comparison of χ^2 from the fits to the PAMELA proton data in two models. The dot indicates the difference of χ^2 between our results and the force-field approximations. The orange line is the smooth result for the scatter points using the Python statsmodels library with the LOWESS (locally weighted scatterplot smoothing) method.

[5] https://www.statsmodels.org

[1] E. N. Parker, Planet. Space Sci. **13**, 9 (1965).
[2] M. Korsmeier and A. Cuoco, Phys. Rev. D **94**, 123019 (2016).
[3] Q. Yuan, S.-J. Lin, K. Fang, and X.-J. Bi, Phys. Rev. D **95**, 083007 (2017).
[4] N. Tomassetti, Phys. Rev. D **96**, 103005 (2017).
[5] J.-S. Niu and T. Li, Phys. Rev. D **97**, 023015 (2018).
[6] J. Wu and C. Huan, Phys. Lett. B **789**, 292 (2019).
[7] Q. Yuan, C.-R. Zhu, X.-J. Bi, and D.-M. Wei, arXiv: 1810.03141.

[8] Q. Yuan, Sci. China Phys. Mech. Astron. **62**, 49511 (2019).
[9] P.-f. Yin, Q. Yuan, J. Liu, J. Zhang, X.-j. Bi, S.-h. Zhu, and X. Zhang, Phys. Rev. D **79**, 023512 (2009).
[10] N. Fornengo, L. Maccione, and A. Vittino, J. Cosmol. Astropart. Phys. 09 (2013) 031.
[11] M. Cirelli, D. Gaggero, G. Giesen, M. Taoso, and A. Urbano, J. Cosmol. Astropart. Phys. 12 (2014) 045.
[12] Q. Yuan, X.-J. Bi, G.-M. Chen, Y.-Q. Guo, S.-J. Lin, and X. Zhang, Astropart. Phys. **60**, 1 (2015).
[13] S.-J. Lin, Q. Yuan, and X.-J. Bi, Phys. Rev. D **91**, 063508 (2015).
[14] S.-J. Lin, X.-J. Bi, P.-F. Yin, and Z.-H. Yu, arXiv:1504.07230.
[15] B. Wang, X. Bi, S. Lin, and P. Yin, Sci. China Phys. Mech. Astron. **61**, 101004 (2018).
[16] E. C. Stone, A. C. Cummings, F. B. McDonald, B. C. Heikkila, N. Lal, and W. R. Webber, Science **341**, 150 (2013).
[17] D. A. Gurnett, W. S. Kurth, L. F. Burlaga, and N. F. Ness, Science **341**, 1489 (2013).
[18] A. C. Cummings, E. C. Stone, B. C. Heikkila, N. Lal, W. R. Webber, G. Jóhannesson, I. V. Moskalenko, E. Orlando, and T. A. Porter, Astrophys. J. **831**, 18 (2016).
[19] P. Picozza *et al.*, Astropart. Phys. **27**, 296 (2007).
[20] M. Boezio *et al.*, New J. Phys. **11**, 105023 (2009).
[21] O. Adriani *et al.*, Astrophys. J. **765**, 91 (2013).
[22] O. Adriani *et al.*, Riv. Nuovo Cimento **40**, 1 (2017).
[23] L. J. Gleeson and W. I. Axford, Astrophys. J. **154**, 1011 (1968).
[24] C. Corti, V. Bindi, C. Consolandi, and K. Whitman, Astrophys. J. **829**, 8 (2016).
[25] I. Cholis, D. Hooper, and T. Linden, Phys. Rev. D **93**, 043016 (2016).
[26] J. Gieseler, B. Heber, and K. Herbst, J. Geophys. Res. **122**, 10964 (2017).
[27] R. Kappl, Comput. Phys. Commun. **207**, 386 (2016).
[28] A. Vittino, C. Evoli, and D. Gaggero, Int. Cosmic Ray Conf. **35**, 24 (2017).
[29] M. J. Boschini, S. Della Torre, M. Gervasi, G. La Vacca, and P. G. Rancoita, Adv. Space Res. **62**, 2859 (2018).
[30] G. Qin and Z.-N. Shen, Astrophys. J. **846**, 56 (2017).
[31] M. S. Potgieter, E. E. Vos, M. Boezio, N. De Simone, V. Di Felice, and V. Formato, Sol. Phys. **289**, 391 (2014).
[32] M. S. Potgieter and E. E. Vos, Astron. Astrophys. **601**, A23 (2017).
[33] M. Orcinha, N. Tomassetti, F. Barão, and B. Bertucci, J. Phys. Conf. Ser. **1181**, 012013 (2019).
[34] N. Tomassetti, F. Barão, B. Bertucci, E. Fiandrini, J. L. Figueiredo, J. B. Lousada, and M. Orcinha, Phys. Rev. Lett. **121**, 251104 (2018).
[35] C. Corti, M. S. Potgieter, V. Bindi, C. Consolandi, C. Light, M. Palermo, and A. Popkow, Astrophys. J. **871**, 253 (2019).
[36] O. P. M. Aslam, D. Bisschoff, M. S. Potgieter, M. Boezio, and R. Munini, Astrophys. J. **873**, 70 (2019).
[37] R. Kappl, Comput. Phys. Commun. **207**, 386 (2016).
[38] M. Martucci *et al.*, Astrophys. J. Lett. **854**, L2 (2018).
[39] G. A. de Nolfo *et al.*, Adv. Space Res. **38**, 1558 (2006).
[40] K. A. Lave *et al.*, Astrophys. J. **770**, 117 (2013).
[41] Y. Shikaze *et al.*, Astropart. Phys. **28**, 154 (2007).
[42] K. Abe *et al.*, Astrophys. J. **822**, 65 (2016).
[43] D. J. McComas, B. L. Barraclough, H. O. Funsten, J. T. Gosling, E. Santiago-Muñoz, R. M. Skoug, B. E. Goldstein, M. Neugebauer, P. Riley, and A. Balogh, J. Geophys. Res. **105**, 10419 (2000).
[44] Y.-M. Wang, N. R. Sheeley, Jr., and N. B. Rich, Geophys. Res. Lett. **27**, 149 (2000).
[45] P. Bobik *et al.*, Astrophys. J. **745**, 132 (2012).
[46] E. N. Parker, Astrophys. J. **128**, 664 (1958).
[47] J. R. Jokipii and J. Kóta, Geophys. Res. Lett. **16**, 1 (1989).
[48] C. W. Smith and J. W. Bieber, Astrophys. J. **370**, 435 (1991).
[49] L. A. Fisk, J. Geophys. Res. **101**, 15547 (1996).
[50] N. Gopalswamy, A. Lara, S. Yashiro, and R. A. Howard, Astrophys. J. Lett. **598**, L63 (2003).
[51] X. Sun, J. T. Hoeksema, Y. Liu, and J. Zhao, Astrophys. J. **798**, 114 (2015).
[52] M. S. Potgieter, Living Rev. Solar Phys. **10**, 3 (2013).
[53] K. Scherer, H. Fichtner, R. D. Strauss, S. E. S. Ferreira, M. S. Potgieter, and H.-J. Fahr, Astrophys. J. **735**, 128 (2011).
[54] R. D. Strauss, M. S. Potgieter, S. E. S. Ferreira, H. Fichtner, and K. Scherer, Astrophys. J. Lett. **765**, L18 (2013).
[55] J. Kóta and J. R. Jokipii, Astrophys. J. **782**, 24 (2014).
[56] B. Heber, H. Fichtner, and K. Scherer, Space Sci. Rev. **125**, 81 (2006).
[57] A. Shalchi, G. Li, and G. P. Zank, Astrophys. Space Sci. **325**, 99 (2010).
[58] N. E. Engelbrecht and R. A. Burger, Astrophys. J. **814**, 152 (2015).
[59] L.-L. Zhao, L. Adhikari, G. P. Zank, Q. Hu, and X. S. Feng, Astrophys. J. **856**, 94 (2018).
[60] J. R. Jokipii, Can. J. Phys. Suppl. **46**, 950 (1968).
[61] J. R. Jokipii, Astrophys. J. **146**, 480 (1966).
[62] J. S. Perko, Astron. Astrophys. **184**, 119 (1987).
[63] M. S. Potgieter and J. A. Le Roux, Astrophys. J. **423**, 817 (1994).
[64] G. Wibberenz, S. E. S. Ferreira, M. S. Potgieter, and H. V. Cane, Space Sci. Rev. **97**, 373 (2001).
[65] R. D. Strauss, M. S. Potgieter, I. Büsching, and A. Kopp, Astrophys. J. **735**, 83 (2011).
[66] N. Tomassetti, F. Barão, B. Bertucci, E. Fiandrini, J. L. Figueiredo, J. B. Lousada, and M. Orcinha, Phys. Rev. Lett. **121**, 251104 (2018).
[67] J. Giacalone and J. R. Jokipii, Astrophys. J. **520**, 204 (1999).
[68] S. E. S. Ferreira and M. S. Potgieter, J. Geophys. Res. **107**, SSH 12-1 (2002).
[69] E. H. Levy, J. Geophys. Res. **81**, 2082 (1976).
[70] J. R. Jokipii, E. H. Levy, and W. B. Hubbard, Astrophys. J. **213**, 861 (1977).
[71] J. R. Jokipii and B. Thomas, Astrophys. J. **243**, 1115 (1981).
[72] R. A. Burger and M. S. Potgieter, Astrophys. J. **339**, 501 (1989).
[73] Y. Yamada, S. Yanagita, and T. Yoshida, Geophys. Res. Lett. **25**, 2353 (1998).
[74] M. Zhang, Astrophys. J. **513**, 409 (1999).
[75] C. Pei, J. W. Bieber, R. A. Burger, and J. Clem, J. Geophys. Res. **115**, A12107 (2010).
[76] A. Ghelfi, F. Barao, L. Derome, and D. Maurin, Astron. Astrophys. **591**, A94 (2016).

[77] C.-R. Zhu, Q. Yuan, and D.-M. Wei, Astrophys. J. **863**, 119 (2018).
[78] O. Adriani *et al.*, Science **332**, 69 (2011).
[79] M. Aguilar *et al.*, Phys. Rev. Lett. **114**, 171103 (2015).
[80] L. Derome, D. Maurin, P. Salati, M. Boudaud, Y. Génolini, and P. Kunzé, Astron. Astrophys. **627**, A158 (2019).
[81] Y. Genolini *et al.*, Phys. Rev. D **99**, 123028 (2019).
[82] M. Boudaud *et al.*, arXiv:1906.07119.
[83] M. S. Potgieter, Adv. Space Res. **13**, 239 (1993).
[84] M. S. Potgieter, R. A. Burger, and S. E. S. Ferreira, Space Sci. Rev. **97**, 295 (2001).
[85] M. S. Potgieter and S. E. S. Ferreira, Adv. Space Res. **27**, 481 (2001).
[86] S. E. S. Ferreira and M. S. Potgieter, Astrophys. J. **603**, 744 (2004).
[87] G. Wibberenz, I. G. Richardson, and H. V. Cane, J. Geophys. Res. **107**, 1353 (2002).
[88] I. G. Usoskin, K. Mursula, S. K. Solanki, M. Schüssler, and G. A. Kovaltsov, J. Geophys. Res. **107**, 1374 (2002).
[89] AMS Collaboration, Phys. Lett. B **494**, 193 (2000).
[90] O. Adriani *et al.*, Astrophys. J. **791**, 93 (2014).